

## Bifunctional ligands for inhibition of tight-binding protein-protein interactions

Taavi Ivan, Erki Enkvist, Birgit Viira, Ganesh babu Manoharan, Gerda Raidaru, Alexander Pflug, Kazi Asraful Alam, Manuela Zaccolo, Richard A. Engh, and Asko Uri

*Bioconjugate Chem.*, **Just Accepted Manuscript** • Publication Date (Web): 07 Jul 2016

Downloaded from <http://pubs.acs.org> on July 7, 2016

### Just Accepted

"Just Accepted" manuscripts have been peer-reviewed and accepted for publication. They are posted online prior to technical editing, formatting for publication and author proofing. The American Chemical Society provides "Just Accepted" as a free service to the research community to expedite the dissemination of scientific material as soon as possible after acceptance. "Just Accepted" manuscripts appear in full in PDF format accompanied by an HTML abstract. "Just Accepted" manuscripts have been fully peer reviewed, but should not be considered the official version of record. They are accessible to all readers and citable by the Digital Object Identifier (DOI®). "Just Accepted" is an optional service offered to authors. Therefore, the "Just Accepted" Web site may not include all articles that will be published in the journal. After a manuscript is technically edited and formatted, it will be removed from the "Just Accepted" Web site and published as an ASAP article. Note that technical editing may introduce minor changes to the manuscript text and/or graphics which could affect content, and all legal disclaimers and ethical guidelines that apply to the journal pertain. ACS cannot be held responsible for errors or consequences arising from the use of information contained in these "Just Accepted" manuscripts.

# Bifunctional ligands for inhibition of tight-binding protein-protein interactions

Taavi Ivan<sup>†</sup>, Erki Enkvist<sup>†</sup>, Birgit Viira<sup>†</sup>, Ganesh babu Manoharan<sup>†</sup>, Gerda Raidaru<sup>†</sup>, Alexander Pflug<sup>‡</sup>, Kazi Asraful Alam<sup>‡</sup>, Manuela Zaccolo<sup>§</sup>, Richard Alan Engh<sup>‡</sup>, Asko Uri<sup>†\*</sup>

<sup>†</sup> Institute of Chemistry, University of Tartu, Tartu, Estonia

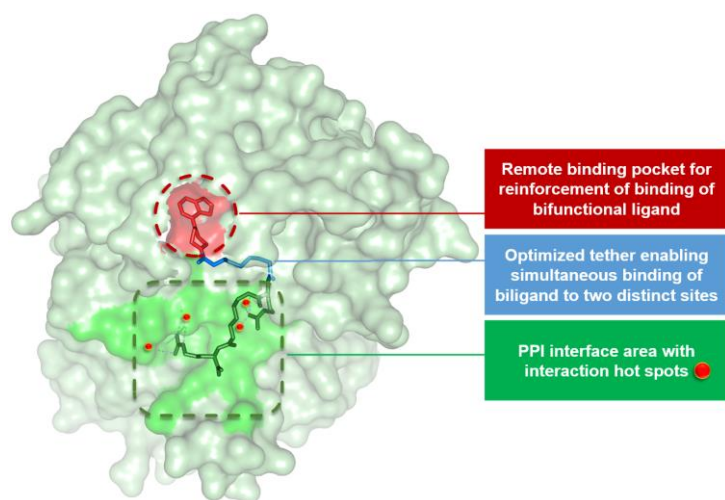
<sup>‡</sup> The Norwegian Structural Biology Centre, Department of Chemistry, University of Tromsø, Tromsø, Norway.

<sup>§</sup> Department of Physiology, Anatomy and Genetics, University of Oxford, Oxford, UK.

**Keywords:** Protein-protein interaction, tight-binding, inhibitor, bisubstrate, bifunctional ligand, protein kinase, PKA holoenzyme, fluorescent probe, fluorescence anisotropy

## Abstract

The acknowledged potential of small-molecule therapeutics targeting disease-related protein-protein interactions (PPIs) has promoted active research in this field. The strategy of using small molecule inhibitors (SMIs) to fight strong (tight-binding) PPIs tends to fall short due to the flat and wide interfaces of PPIs. Here we propose a biligand approach for disruption of strong PPIs. The potential of this approach was realized for disruption of the tight-binding ( $K_D = 100$  pM) tetrameric holoenzyme of cAMP-dependent protein kinase (PKA). Supported by X-ray analysis of co-crystals, bifunctional inhibitors (ARC-inhibitors) were constructed that simultaneously associated with both the ATP-pocket and PPI interface area of the catalytic subunit of PKA (PKAc). Bifunctional inhibitor ARC-1411, possessing  $K_D$  value of 3 pM towards PKAc induced the dissociation of the PKA holoenzyme with a low-nanomolar  $IC_{50}$ , whereas the ATP-competitive inhibitor H89 bound to the PKA holoenzyme without disruption of the protein tetramer.



## Introduction

Estimates of the number of protein-protein interactions (PPI) comprising the “human interactome” have increased from a few thousands in 1995 up to 650 000 in 2013.<sup>1,2</sup> This is in sharp contrast to a gradual decrease of the number of human protein-coding genes (19000 genes).<sup>3</sup> The functional interactome has been a key focus of disease-related protein network characterization, with the ultimate goal to enable therapeutic control of PPIs with small-molecule inhibitors (SMIs). Currently, 50 PPIs have been proposed as potential targets for drug intervention, and 22 corresponding SMIs have reached phase I/II clinical trials.<sup>4</sup>

Stabilities of protein complexes vary broadly with the values of dissociation constant ( $K_D$ ) ranging from low mM to single-digit pM, whereas the majority of the  $K_D$ -s fall into micromolar and nanomolar range.<sup>5</sup> The contact surfaces of PPIs usually cover large flat areas (1500 to 3000 Å<sup>2</sup>),<sup>5</sup> thus SMIs can effectively target PPIs only *via* interaction with key amino acid residues (hot spots) that are critically important for stability of the complex.<sup>6</sup> Classical high throughput screening, fragment-based drug design, and virtual screening usually identify PPI inhibitors with micromolar affinities,<sup>2</sup> whereas inhibitors with higher affinity are required for disruption of tight-binding ( $K_D < 200$  nM) protein complexes.<sup>7,8</sup> Furthermore, a SMI that disrupts the PPI in a biochemical assay may fail in cells either due to inadequate uptake of the SMI, degradation of the SMI in biological milieu, or because the PPI is reinforced in complex cellular environment.

Signaling networks obviously employ many PPIs, of which interactions of protein kinases (PKs) with its substrates are a part.<sup>9</sup> Dysregulation of phosphorylation of proteins is associated with cancers, inflammatory disorders, diabetes, and other diseases; as a consequence, this family of enzymes has come to constitute one of the most important drug target class over the past two decades.<sup>10</sup> All small-molecule PK inhibitors currently approved by FDA as cancer drugs bind to the deep and largely hydrophobic ATP-pocket of the PK. However, high conservation of the nucleotide-binding site across more than 500 human PKs presents a challenge for the construction of PK inhibitors that are suitable for specific therapeutic and research applications. Nevertheless, as an indication of the success of cancer drug development efforts, more than 30 small-molecule PK inhibitors have been approved for clinical use.<sup>11</sup>

By definition, all PKs inevitably participate in PPIs: the bisubstrate mechanism of the PK-catalyzed protein phosphorylation reaction involves formation of the molecular triple complex incorporating the PK, a substrate protein, and ATP. Usually the interactions between PKs and protein substrates are relatively weak, possessing  $K_D$ -s in micromolar range.<sup>12</sup> In

addition to catalytic functions, PKs also possess non-catalytic functions, e.g. protein scaffolding.<sup>13</sup> Even more, 10% of human PKs are “pseudokinases” that possess no or weak catalytic activity.<sup>13,14</sup> Thus, PPIs play dual roles in case of PKs. From one side, functioning (activity and localization in cells) of PKs is regulated by PPIs. On the other hand, PKs regulate the functioning of the target proteins through specific PPIs. Taken together, the development of inhibitors of PPIs offers a promising approach for the selective regulation of activity of PKs in cells.

cAMP-dependent protein kinase (PKA) has been used as a prototype enzyme for large and highly diverse protein super-family of PKs.<sup>15</sup> PKA is a ubiquitous intracellular cAMP effector that regulates the functioning of many intracellular proteins and plays a critical role in the integration of signaling networks in eukaryotic cells. The activity and localization of PKA are regulated through a complicated PPI network in a multiprotein hetero-complex that comprises 5 proteins: two catalytic subunits of PKA (PKAc) and a dimer of regulatory subunits [(PKAr)<sub>2</sub>] form the PKA holoenzyme, that is bound to an A-kinase anchoring protein (AKAP). At low cAMP concentrations the PKA/AKAP hetero-complex is held together by a network of strong PPIs that cause the dimerization of PKAr, association of PKAr dimer with AKAP ( $K_D$ -s ranging from low nanomolar for PKArII to 200 nM for PKArI),<sup>16</sup> and interaction of two PKAc monomers with (PKAr)<sub>2</sub> that leads to a stable ( $K_D$  = 100 – 200 pM) PKA holoenzyme.<sup>17</sup>

Disruption of strong protein complexes possessing  $K_D$ -s in picomolar range requires the application of inhibitors with very high affinity towards any of the proteins participating in the complex formation. Moreover, the protein-bound inhibitor should at least partially cover the contact area of the PPI for disruption of the protein complex. An acknowledged technology for the construction of high-affinity inhibitors works through incorporation of several fragments that interact with separated binding regions (“pockets”) of the target protein.<sup>18,19</sup> The binding of a protein with a bifunctional (bivalent) ligand composed of two covalently tethered monofunctional ligands may lead to a very stable ligand:protein complex ( $K_D$  value in the picomolar range). In case the bifunctional inhibitor retains the interactions of each individual fragment upon complexing with the protein, the binding free energy for the bifunctional inhibitor is equal to the sum of binding free energies of the monofunctional fragments, plus an entropic gain resulting from the interaction of a single molecule rather than multiple fragments with the protein molecule.<sup>20</sup>

Previously, we have used the bifunctional approach for the development of high-affinity bisubstrate inhibitors for several PKs: PKAc, CK2, PIM1, ROCK, Haspin, etc.<sup>21,22</sup> In the

1  
2  
3 91 present work, supported by structure-affinity studies and X-ray analysis of inhibitor:PK co-  
4  
5 92 crystals, we developed bifunctional ARC-inhibitors whose affinity towards PKAc extended to  
6  
7 93 one-digit picomolar range ( $K_D = 3$  pM). Area of binding of PKAc with ARC-compounds partly  
8  
9 94 overlaps with the contact area of interaction of PKAc with PKAr, making possible the  
10  
11 95 disruption of the protein tetramer of PKA holoenzyme with ARCs. This result demonstrates  
12  
13 96 that bifunctional ligands possessing very high (picomolar) affinity towards a partner protein of  
14  
15 97 PPI complex can disrupt stable PPI complexes, provided that the SMI interaction overlaps with  
16  
17 98 the area of hot spot interactions.  
18  
19  
20  
21  
22  
23  
24  
25  
26  
27  
28  
29  
30  
31  
32  
33  
34  
35  
36  
37  
38  
39  
40  
41  
42  
43  
44  
45  
46  
47  
48  
49  
50  
51  
52  
53  
54  
55  
56  
57  
58  
59  
60

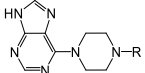
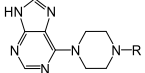
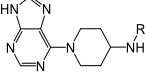
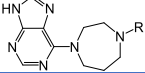
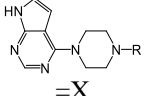
Results

Characterization of 7-deazapurine-based bifunctional inhibitors

Affinities of synthesized inhibitors towards PKAα, AKT3, and ROCKII

A new set of ARC-compounds was designed proceeding from the previously reported lead compound ARC-670, because of its high affinity ( $K_D = 0.82$  nM) and good crystal-forming ability with PKAα.<sup>23</sup> Structures of ARCs together with their affinities towards PKs PKAα, AKT3, and ROCKII are listed in Table 1.

Table 1. Structures of ARCs and their affinities towards PKs PKAα, AKT3, and ROCKII

compound code	nucleosidic moiety	linker region	peptidic moiety	$K_D$ , nM (95% CI)		
				PKAα	AKT3	ROCKII
ARC-902 <sup>a</sup>				0.32 (0.26–0.36)	39 (32–50)	1.56 (1.35–1.81)
ARC-670 <sup>b</sup>		Oda	(DArg) <sub>6</sub> -NH <sub>2</sub>	0.82	8.4	nd
ARC-1403		Oda	DArg-NH <sub>2</sub>	171 (127–230)	2593 (2075–3241)	392 (285–539)
ARC-1156		Oda	DArg-NH <sub>2</sub>	578 (468–715)	10990 (8440–14320)	1398 (947–2062)
ARC-1169		Oda	DArg-NH <sub>2</sub>	735 (543–995)	6421 (4737–8700)	1620 (1330–1975)
ARC-1404		Oda	DArg-NH <sub>2</sub>	29 (26–33)	430 (350–533)	48 (34–67)
ARC-1407	X-	Hda	DArg-Ahx-DArg-NH <sub>2</sub>	4.6 (4.2–5.1)	107 (91–123)	53 (43–66)
ARC-1408	X-	Nda	DArg-Ahx-DArg-NH <sub>2</sub>	0.18 (0.17–0.20)	9.5 (8.5–10.6)	3.9 (3.4–4.4)
ARC-1409	X-	Nda	DArg-NH <sub>2</sub>	1.7 (1.5–2.0)	41 (30–52)	9.3 (7.9–10.8)
ARC-1410	X-	Dda	DArg-NH <sub>2</sub>	12 (10–15)	171 (132–222)	26 (21–31)
ARC-1411	X-	Nda	(DArg) <sub>6</sub> -DLys-NH <sub>2</sub>	0.0030 (0.0025–0.0041)	0.31 (0.24–0.41)	0.030 (0.015–0.055)
ARC-1412	X-	Nda	(DArg) <sub>6</sub> -DLys (COC <sub>13</sub> H <sub>27</sub> )-NH <sub>2</sub>	0.035 (0.030–0.041)	32 (27–39)	3.5 (3.2–3.9)
ARC-1413	X-	Nda	(DArg) <sub>6</sub> -DLys (5-TAMRA)-NH <sub>2</sub>	0.0054 (0.0045–0.0065)	2.9 (2.7–3.3)	1.18 (1.00–2.40)
ARC-1414	X-	Nda	DLys-NH <sub>2</sub>	4.2 (3.6–4.9)	410 (268–628)	7.8 (6.4–9.4)
ARC-1415	X-	Nda	(DArg) <sub>6</sub> -NH <sub>2</sub>	0.0062 (0.0053–0.0072)	0.84 (0.74–0.92)	0.22 (0.18–0.27)
ARC-1416	X-	Nda	DAla-(DArg) <sub>5</sub> -NH <sub>2</sub>	0.0095 (0.0086–0.0104)	2.8 (1.9–4.1)	1.54 (1.03–2.26)

<sup>a</sup>Reference compound, affinity determined previously<sup>24,25</sup>; <sup>b</sup>Lead compound<sup>23</sup>; nd – not determined; Ahx, 6-aminohexanoic acid; Dda, α,ω-decanedioic acid; Hda, α,ω-heptanedioic acid; Nda, α,ω-nonanedioic acid; Oda, α,ω-octanedioic acid. Full structures, HRMS data, and experimental displacement curves in Supporting Information Part 2-4.

ARC-670 and newly synthesized ARCs contain  $\alpha,\omega$ -diacid linker between the peptide fragment and the adenosine-mimicking moiety (Table 1). ARC-1403 incorporating a single D-arginine was synthesized according to a new synthetic pathway (please see **Supporting Information Part 1, Figure S1**), allowing the performance of measurements in a convenient range of affinity. Three fragments were identified whose modification potentially leads to increase of affinity of the conjugates towards AGC kinases: piperazine fragment, purine moiety, and length of the linker.<sup>23,25</sup>

First, the effect of piperazine moiety was tested. Crystal structure of ARC-670 revealed no polar interactions between PKA $\alpha$  and piperazine or its adjacent carbonyl group.<sup>23</sup> However, replacement of piperazine in the structure of ARC-1403 with 4-aminopiperidine (ARC-1156) or homopiperazine (ARC-1169) caused several-fold decrease in affinity towards the tested PKs. Piperazine seemed to allow favorable placement of the subsequent structure in the glycine-rich loop of PKs, and was therefore retained as a structural element in modified ARCs.

Second, we substituted 7-deazapurine for purine, obtaining ARC-1404. While the crystal structure of ARC-670:PKA $\alpha$ <sup>23</sup> showed that N7 of the purine ring could be the acceptor atom for the hydrogen bond with Thr183, ARC-1404 revealed 6-fold increase in affinity towards both PKA $\alpha$  and AKT3, compared to ARC-1403. Therefore, we used 7-deazapurine fragment as ATP binding site-directed motif in further structural optimizations.

Third, proceeding from ARC-1404, the length of the linker was adjusted. Analogues of ARC-1404 were synthesized comprising  $\alpha,\omega$ -heptanedioic acid (ARC-1407),  $\alpha,\omega$ -nonanedioic acid (ARC-1408 and ARC-1409), or  $\alpha,\omega$ -decanedioic acid (ARC-1410) linker. Within the structures of ARC-1407 and ARC-1408, additional linker of 6-aminohexanoic (Ahx) acid was incorporated for positioning of the following D-arginine residue(s) farther away from the D-arginine spacer. Comparison of  $K_D$  values of ARC-1404, ARC-1407, ARC-1408, ARC-1409, and ARC-1410 towards tested PKs (**Figure S2A**) revealed that the application of  $\alpha,\omega$ -nonanedioic acid linker leads to the highest affinity of the compounds, with a strong dependency of only an atom-length difference of the linker.

We have previously established that six D-arginine residues in the peptide moiety led to substantial gain in affinity of ARCs towards basophilic PKs.<sup>18</sup> The number of D-arginine residues in the peptide part of ARC-1409 was increased, leading to compounds ARC-1411, ARC-1415, and ARC-1416 (Table 1). These conjugates revealed almost 1000-fold higher affinity towards PKA $\alpha$  than ARC-1409. Comparison of affinity of ARC-1411, ARC-1415,

and ARC-1416 showed that ROCKII affinity of ARCs was especially sensitive to the composition of peptide moiety (50-fold reduction from ARC-1411 to ARC-1416) (**Figure S2B**). Amongst these inhibitors, ARC-1411 was the superior binder possessing  $K_D$  value of 3 pM towards PKA $\alpha$ , 310 pM towards AKT3, and 30 pM towards ROCKII. The fluorescent probe ARC-1413, obtained by labeling of ARC-1411 at D-lysine residue with the fluorescent dye 5-TAMRA, retained very high affinity ( $K_D = 5.6$  pM) of the unlabeled parent compound towards PKA $\alpha$ .

The inhibitory potency of ARC-1411 was tested at 1  $\mu$ M concentration towards 93 PKs in a commercial panel. Great majority of basophilic kinases were inhibited by more than 75% (**Table S1**) whereas non-basophilic PKs such as CK2, PLK1, and GSK3 were not inhibited.

#### ***Correlation of $K_D$ values and ThermoFluor $\Delta T_m$ values for ARC:PKA $\alpha$ complexes***

$K_D$  values found from the time-resolved (TR) luminescence binding/displacement assay<sup>26</sup> were compared to  $\Delta T_m$  values from ThermoFluor-based<sup>27</sup> PK denaturation stabilizing effect for inhibitors comprising the same nucleoside moiety. The similar trends in dependency of  $\Delta T_m$  values on the structure of ARCs were established for PKA $\alpha$  and AKT3 (**Figure S3**). For comparison,  $\Delta T_m$  value of 6.8  $^{\circ}$ C was determined for Hidaka's inhibitor H89<sup>28</sup> towards PKA $\alpha$ , well-coinciding with previously published  $\Delta T_m$  value of 6.9  $^{\circ}$ C.<sup>29</sup>

Inhibitors ARC-1411, ARC-1415, and ARC-1416 revealed the strongest stabilizing effect towards PKA $\alpha$  with  $\Delta T_m$  values of 17.1  $^{\circ}$ C, 16.2  $^{\circ}$ C, and 16.7  $^{\circ}$ C, respectively, that all substantially surpassed the previously reported highest  $\Delta T_m$  value of 11.3  $^{\circ}$ C for the generic PK inhibitor staurosporine towards PKA $\alpha$ .<sup>29</sup>

Correlation of  $\Delta T_m$  values with inhibition constants or isothermal titration calorimetry (ITC) data have been published previously,<sup>30–32</sup> now we correlated  $\Delta T_m$  values with the  $K_D$  values determined in the binding/displacement assay with TR luminescence intensity read-out. **Figure 1** shows a good linear dependency ( $R^2 = 0.97$ ) between  $\Delta T_m$  and  $pK_D$  values for association of the tested ARC-based inhibitors with PKA $\alpha$ . Linear analysis of the  $pK_D$ – $\Delta T_m$  plot revealed the  $pK_D$  value at which linear regression graph intercepted abscissa, pointing to the real concentration of the active form of PKA $\alpha$  (7.2  $\mu$ M of total 10  $\mu$ M) in the ThermoFluor assay.



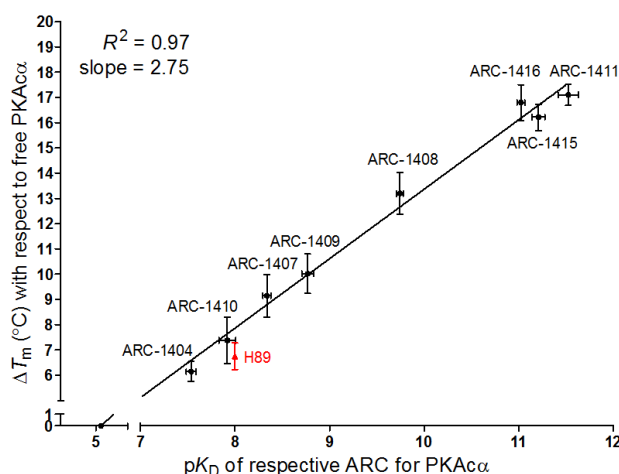


**Figure 1. Correlation between  $K_D$  values and ThermoFluor  $\Delta T_m$  values.** Linear plot of inhibitor-induced thermal denaturation temperature change ( $\Delta T_m$ ) and a negative logarithm of corresponding dissociation equilibrium constants ( $pK_D$ ) for inhibitor:PKA $\alpha$  complexes.

### ***Dissociation kinetics of ARC-1413 from its complex with PKA $\alpha$***

We have shown that ARC-based inhibitors and photoluminescent probes associate with target PKs with near diffusion-limited association kinetics.<sup>33</sup> Regarding the similar structure and binding mechanism of the ARCs described here, the association kinetics is not expected to vary significantly between ARCs. Therefore, change in equilibrium dissociation constant of the ARC:PK complexes is mainly attributed ( $K_D = k_{off}/k_{on}$ ) to the decrease in dissociation rate constant. We measured the dissociation half-life of the complex of fluorescent probe ARC-1413 and PKA $\alpha$  ( $K_D = 5.6$  pM). Following the dissociation kinetics in the presence of a competing inhibitor ARC-1411 or ARC-902 in an assay with fluorescence anisotropy (FA) read-out revealed the dissociation half-life of 17.7 min for the complex of ARC-1413:PKA $\alpha$  (Figure S4).

### **Disruption of a picomolar PPI complex with bifunctional ARC-inhibitors**

#### ***Application of the fluorescent probe ARC-1413 for characterization of strong PPIs involving PKAc***

The fluorescent probe ARC-1413 was used to determine the affinity of natural regulators of PKA activity, heat-stable PKA inhibitor protein PKI $\alpha$ <sup>34,35</sup> and PKArI $\alpha$ , towards the enzyme PKA $\alpha$  (Figure 2).  $K_D$  values of 0.22 (0.16–0.29) nM and 62 (53–73) pM were determined for complexes PKI:PKA $\alpha$  and PKArI $\alpha$ :PKA $\alpha$ , respectively [ $K_D = 43 \pm 7$  pM has been reported for PKArI $\alpha$ :PKA $\alpha$  on the basis of surface plasmon resonance (SPR) measurements].<sup>36</sup> The latter titration series was subsequently treated with cAMP (final

concentration of 50  $\mu$ M) to induce the dissociation of holoenzyme and rebinding of ARC-1413 to PKA $\alpha$  (Figure 2,■).

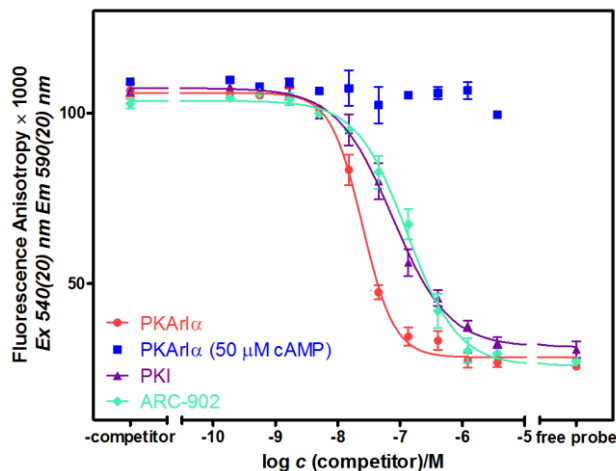


**Figure 2. Determination of affinity of inhibitors towards PKA $\alpha$ .** Displacement of the probe ARC-1413 (2 nM) from PKA $\alpha$  (3 nM total active concentration) with control (ARC-902, ◆), PKI (▲), or PKArl $\alpha$  (●), and subsequent liberation of catalytic subunit from the latter by cAMP (■) as detected by measurement of FA.

**Displacement of PKArl $\beta$ -CFP from complex with PKA $\alpha$ -YFP by ARC-1411**

Genetically engineered variant of a cAMP-sensor that is based on the measurement of intensity of non-radiative Förster-type resonant energy transfer (FRET) between two interacting fluorophores positioned in close proximity, lysate of cells expressing the fusions of cyan fluorescent protein (CFP) and yellow fluorescent protein (YFP) with PKAr and PKAc,<sup>37,38</sup> respectively, was used for gaining direct evidence that ARC-based biligands disrupt the interaction between regulatory and catalytic subunits of PKA. Lysate of C9H6 cells (CHO cells stably expressing fusion proteins PKArl $\beta$ -CFP and PKA $\alpha$ -YFP) was separated and diluted 20-fold (characterization of lysate in Supporting Figure S5). Disruption of the tetrameric PKA holoenzyme was induced by cAMP, which led to cease of FRET. The  $EC_{50}$  value of 48 nM was determined for activation of PKA by cAMP (Figure 3B,▲). The activation constant ( $K_a$ ) of 580-600 nM has been previously reported for cAMP activation of full-length PKA holoenzyme (PKArl $\beta$ :PKAc) as determined by kemptide phosphorylation activity, while the value of  $K_a$  is 10-fold higher than the affinity of cAMP towards PKArl $\beta$  ( $K_{D,cAMP}$  = 60 nM).<sup>39</sup>

Thereafter we tested the potential of two ARC-based bifunctional inhibitors, ARC-1411 and ARC-902 to disrupt PKA holoenzyme (Figure 3A).  $IC_{50}$  values of 2 nM and 109 nM were obtained for displacement of PKArl $\beta$  by ARC-1411 and ARC-902, respectively (Figure 3B). In the presence of ATP and  $Mg^{2+}$  the lower plateau of 530/480 FI ratio decreased for the ARC-1411 and ARC-902, resembling the effect seen for cAMP without the presence of  $Mg^{2+}$ /ATP

(Figure 3C). Addition of  $Mg^{2+}$ /ATP induced slight increase in the upper plateau value for the titration series of both cAMP and ARC-inhibitors, with primary effector identified as  $Mg^{2+}$  rather than ATP (Figure S6A). It is expected that a lysate contains nucleotides that apply cations as cofactors in binding to the active site, which induces the conformational packing of the enzyme. Binding of H89 to PKA $\alpha$  revealed no cooperativity with  $Mg^{2+}$ , this result is in accord with results of NMR analysis.<sup>40</sup> Furthermore, the removal of  $Mg^{2+}$  with 20 mM EDTA had no effect to the FRET between PKA $\beta$ -CFP:PKA $\alpha$ -YFP in the presence of H89, while in the absence of both  $Mg^{2+}$  and H89 the maximum FRET efficiency decreased (Figure S6B). The displacement curves for ARC-1411 and ARC-902 are shifted in the presence of competitive ATP (100  $\mu$ M), resulting in  $IC_{50}$  values of 22 nM and 2.4  $\mu$ M, respectively. The influence of ATP to the cAMP titration series is smaller leading to 45% increase in the value of  $EC_{50}$  ( $EC_{50,cAMP}$  = 68 nM), comparable to the previously reported value of 60 nM.<sup>39</sup>

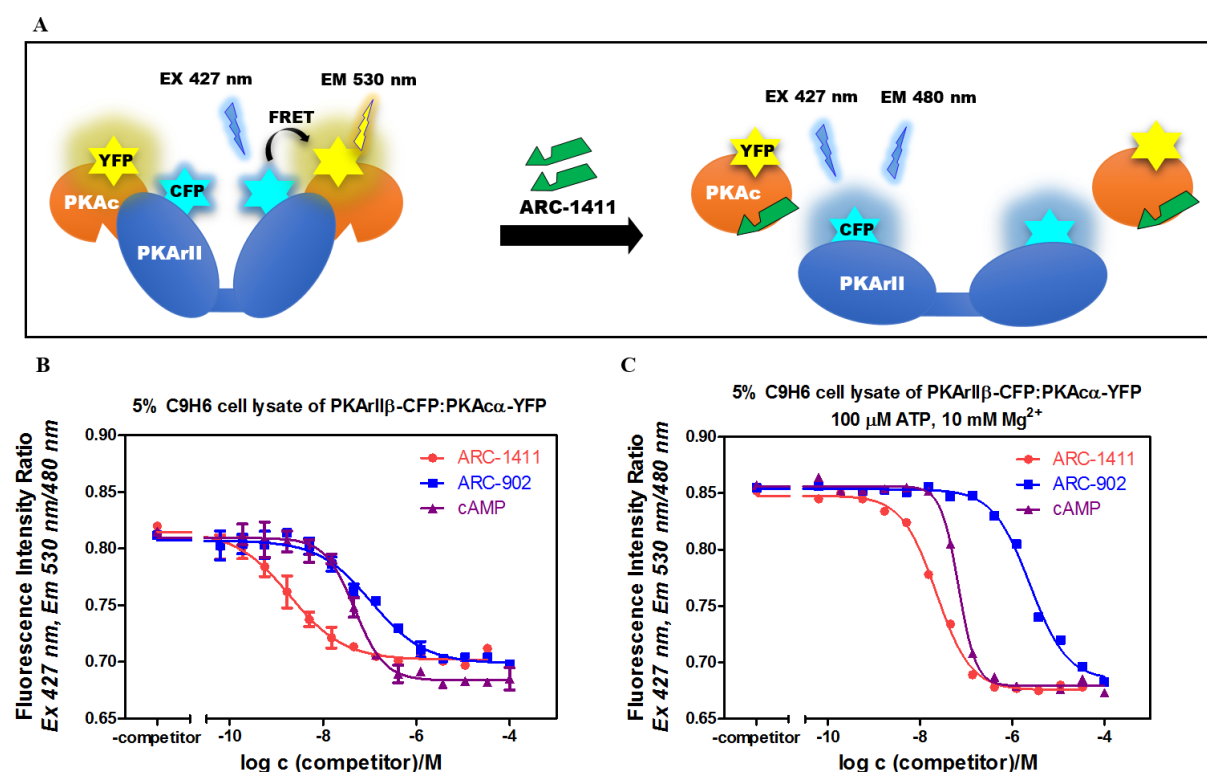


**Figure 3. Disruption of PKA holoenzyme by PKA activator cAMP and ARC-inhibitors.** (A) Scheme of disruption of the complex of CFP-fused PKAII $\beta$  (blue) and YFP-fused PKA $\alpha$  (orange) by ARC-1411 (green), leading to interruption of FRET and decrease in the ratio of fluorescence intensities in 530 nm and 480 nm channels. (B) Titration 5% lysate of C9H6 cells expressing PKAII $\beta$ -CFP and PKA $\alpha$ -YFP with cAMP (▲), ARC-1411 (●), and ARC-902 (■). (C) Experiments were performed as in B, in the presence of ATP (100  $\mu$ M) and  $Mg^{2+}$  (10 mM).

### Association of H89 with PKA holoenzyme

Previous X-ray analysis of the co-crystals of H89:PKA $\alpha$ :PKI(5-24) triple complex, in which H89 and PKI peptide PKI(5-24) are simultaneously associated with PKA $\alpha$ , revealed lack

of direct interaction between the two ligands.<sup>41,42</sup> On the other hand, to the best of our knowledge, there is no direct evidence available whether H89 could bind to PKA holoenzyme without disrupting the tetrameric structure. H89 is a small-molecule generic inhibitor of PKs of the AGC group that with high affinity ( $K_D = 10$  nM)<sup>33</sup> binds to the ATP-pocket of PKAc. As the positioning of H89 in the ATP-pocket is different from that of  $Mg_2ATP$ , it is not clear whether H89 can also bind into ATP-pocket of PKAc in the tetrameric PKA holoenzyme.

Here we investigated the effect of H89 on PKA holoenzyme that was constituted of fluorescent fusion proteins PKA $\beta$ -CFP and PKA $\alpha$ -YFP in lysate of C9H6 cells. After inducing the dissociation of the holoenzyme with the bisubstrate inhibitor ARC-902, H89 was added to the solution in excess (Figure 4A). We hypothesized that ARC-902 ( $K_{D,PKA\alpha} = 0.32$  nM)<sup>24</sup> disrupts the PKA holoenzyme by associating with PKA $\alpha$ -YFP, leading to cancellation of FRET. At higher concentrations H89 would displace ARC-902 from PKAc and the H89:PKAc complex in turn associates with PKA $\beta$ . This formation of PKA holoenzyme complex, that comprises two H89 molecules, would lead to recurrence of FRET between the fluorescent proteins.

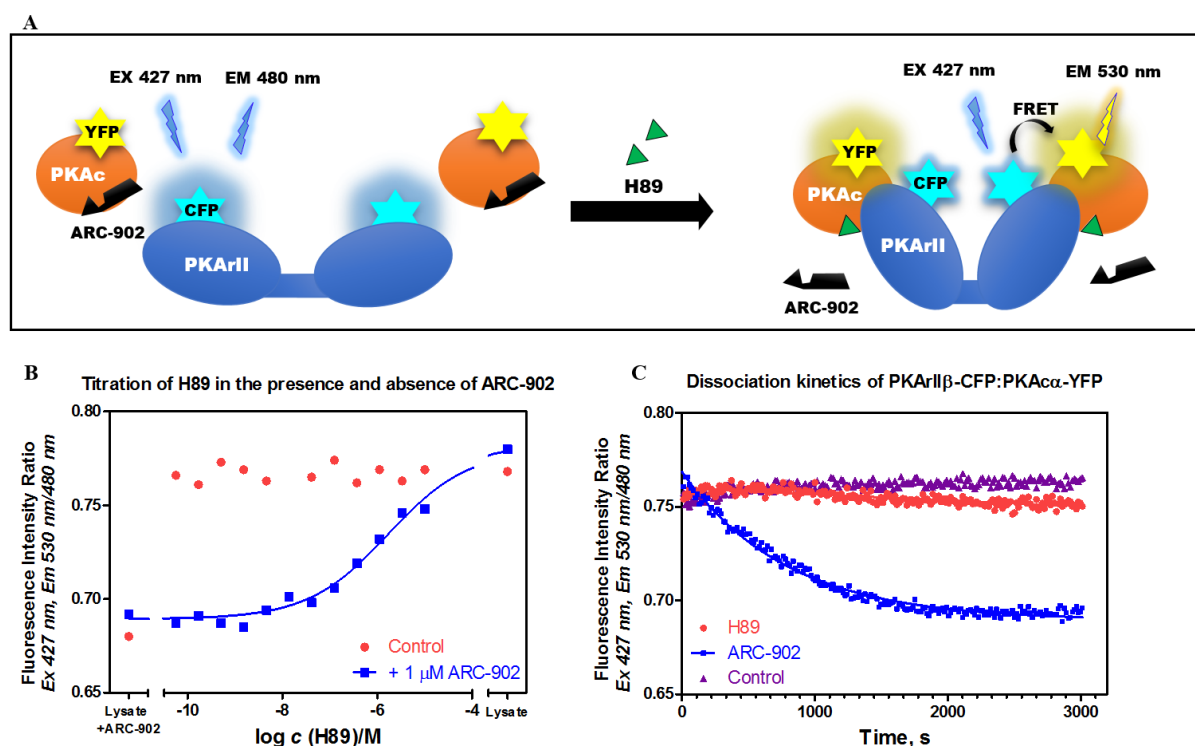


**Figure 4. FRET assay for PKA holoenzyme dissociation.** (A) Scheme of the proposed process of displacement of a PKA $\beta$ -competitive bisubstrate probe ARC-902 (black) from PKA $\alpha$  (orange) by H89 (green), leading to PKA holoenzyme reformation and accompanying increase in FRET from CFP to YFP. (B) Dilution series of H89 in the absence (●) and presence (■) of 1  $\mu$ M ARC-902. (C) Dissociation kinetic profiles of PKA $\beta$ -CFP:PKA $\alpha$ -YFP with addition of ARC-902 (10  $\mu$ M, ■) or H89 (50  $\mu$ M, ●) at  $t=0$ .

Steady-state fluorescence intensity measurements revealed that H89 could not disrupt PKA holoenzyme as there was no decrease in FRET even at 10  $\mu$ M concentration of H89 (Figure 4B,●). Simultaneous association of H89 ( $K_{D,PKA\alpha} = 10$  nM)<sup>33</sup> and PKArII $\beta$ -CFP with PKA $\alpha$ -YFP was confirmed by using bisubstrate inhibitor ARC-902 at 1  $\mu$ M concentration. ARC-902 disrupted the PKA holoenzyme by displacing PKArII $\beta$ -CFP from PKA $\alpha$ -YFP, leading to cancellation of FRET between the fluorescent proteins (Figure 4B,■). At higher concentrations H89 replaced ARC-902 in complex with PKA $\alpha$ -YFP, liberating the protein for association with PKArII $\beta$ -CFP (Figure 4B,■).

We then questioned whether H89 has to displace PKArII $\beta$  before the formation of H89 complex with holoenzyme. H89 was added to the lysate containing PKArII $\beta$ -CFP:PKA $\alpha$ -YFP and the FI ratio (FI530/FI480) was monitored in time. H89 bound to the ATP-pocket without prior disruption of the interactions between PKArII $\beta$ :PKA $\alpha$  (Figure 4C,●), as the FRET remained constant within observed time interval. In comparison, ARC-902 induced the dissociation of PKA holoenzyme (Figure 4C,■), resulting in  $k_{off}$  value of  $1.27 \cdot 10^{-3} \text{ s}^{-1}$ . This value is close to the reported values of dissociation rate constants that range from  $1.23 \cdot 10^{-3} \text{ s}^{-1}$  to  $2.6 \cdot 10^{-4} \text{ s}^{-1}$  for different variants of PKArII $\beta$ :PKA $\alpha$  as measured with SPR spectroscopy.<sup>43,44</sup>

### **X-ray analysis of co-crystals of complexes of PKA $\alpha$ with ARC-1408, ARC-1411, and ARC-1416**

According to X-ray analysis the structure of PKA $\alpha$ :ARC-1408 co-crystal features one protein molecule in the asymmetric unit, well defined by electron density from Glu13 to Phe350 (Figure 5A). Positioning of ARC-1408 in the active site of PKA $\alpha$  clearly points to the bifunctional character of the compound. Binding sites of both substrates of the PK are involved into interactions with ARC-1408: contacts with ARC-1408 are visible for Glu121 and Val123 in the ATP-binding site,<sup>45</sup> but also for Asp166, Glu170, and Glu230 in the hot spots region of PPI interface of PKArII $\beta$ :PKA $\alpha$  association.<sup>15,39</sup> Additional interactions of the linking region with residues Phe54 and Ser53 are also apparent.

Co-crystal of ARC-1411:PKA $\alpha$  holds two mirror-imaged protein molecules in the asymmetric unit. The protein molecules face each other with their active sites, which in both cases are occupied by a single ARC-1411 molecule. Six D-arginines of ARC-1411 seem to allow multiple binding modes to the substrate binding site of PKA $\alpha$  resulting in unclear electron density (excluded from the model) beyond D-Arg3 for the ARC compound in chain B (Figure S7B), and D-Arg2 for the ARC compound in chain A (Figure S7A). ARC-1411 induces the ATP-pocket to adapt the open conformation only seen with the compound ARC-



1012 (PDB entry 3AG9)<sup>23</sup>. The catalytic activity of PKA $\alpha$  is attributed to phosphorylation of Thr197, which then interacts with His87 for stabilization of the activation loop. Both structures with ARC-1411 (chain A and chain B) are characterized by a strong shift of His87, abolishing the interaction with pThr197 in the activation loop (**Figure S7C**). Unlike to the structure 3AG9, where His87 shows no interactions to other residues, His87 in ARC-1411:PKA $\alpha$  co-crystal interacts with Gly187 in the DFG-motif.

Within ARC-1416, D-Arg3 offers multiple conformations and the terminal D-Arg reveals unclear electron density. Well-defined interactions with PKA $\alpha$  are formed for D-Arg2 (interacts with Glu127) and D-Arg4 (with Glu170 and Glu230). Differently from ARC-1411-induced open conformation of glycine-rich flap of PKA $\alpha$ , D-Ala residue in the pos1 of peptidic moiety of ARC-1416 allows the glycine-rich flap to adapt the intermediate conformation as in ARC-1408:PKA $\alpha$  complex (**Figure 5B**).

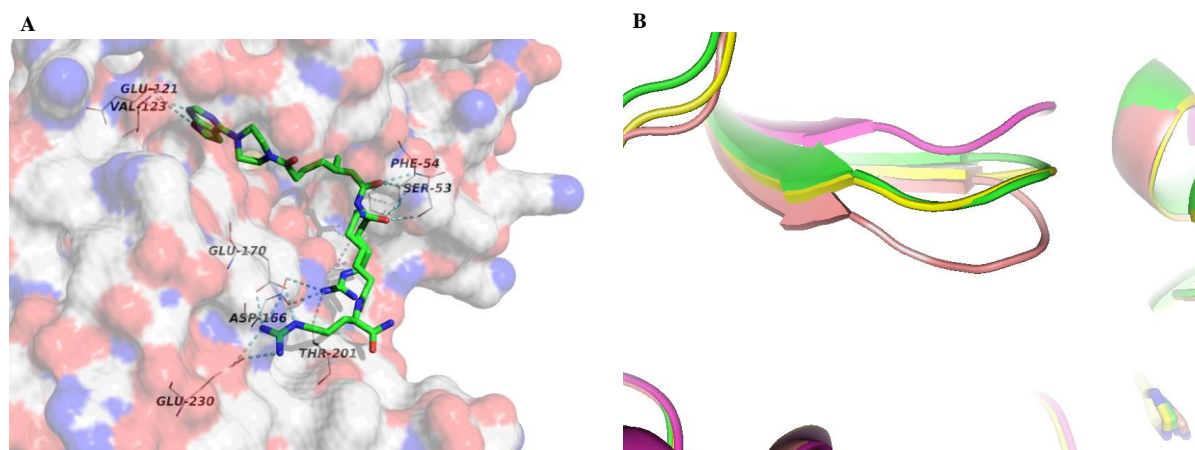


**Figure 5. Crystal structure analysis of ARC:PKA $\alpha$  complexes.** (A) ARC-1408 in the active site of PKA $\alpha$ . Amino acid residues within PKA $\alpha$  forming hydrogen bonds with ARC-1408 are depicted. (B) Overlay of PKA $\alpha$  co-crystal structures with ARC-1408 (green), ARC-1411 (pink), ARC-1416 (yellow), and inhibitor peptide (light brown, PDB entry 2CPK) showing conformational differences in the glycine-rich flap: closed (2CPK), intermediate (ARC-1408, ARC-1416), and open state (ARC-1411).

## Discussion

SMIs of specific PPIs have been acknowledged as potential therapeutic agents. On the other hand, “Lipinski’s rule of five”<sup>46</sup> may be not the best guideline to effective small drugs for disruption of protein complexes<sup>47</sup>. Shallow and extensive contact area of a tight-binding PPI interface implies that an effective inhibitor should comprise multiple pharmacophoric elements positioned dispersedly for interaction with hot spots of the target protein. Therefore, MW limit of 500 D may be insufficient to mount the minimal number of pharmacophoric elements for achieving adequate affinity of the compound towards the protein involved in the PPI.

In this study the biligand approach was used for the rational development of disruptors of tight-binding protein complexes. A new synthetic scheme was established for synthesis of conjugates of heteroaromatic systems and peptide analogs (ARCs). The peptide moiety of an ARC interacts with the contact surface involved in PPI and the strength of this interaction is reinforced through binding of “affinity hook” of the ARC to a specific binding pocket (e.g., ATP-pocket) of the interacting protein. Supported by the results of X-ray analysis of ARC:PKAc co-crystals and extensive structure-affinity studies, bifunctional PKAc inhibitors were developed whose affinity extended down to low picomolar range. These ARC-inhibitors disrupted the tight-binding PKA holoenzyme complex by associating with PKAc.

The fluorescent probe ARC-1413 ( $K_{D,PKAc\alpha} = 5.6$  pM) was employed in a simple homogeneous assay with FA read-out for the investigation of a tight-binding protein complex, PKA holoenzyme, possessing  $K_D$  value of 100 pM<sup>36,43</sup>. Characterization of such strong PPIs requires the application of very high-affinity probes, as the  $K_D$  value of the probe determines the lowest  $K_D$  value of the PPI complex that can be reliably established in the FA-based assay.<sup>48</sup> The homogeneous fluorescence-based assay is less labor- and material-consuming than ITC- and SPR-based methods. Other methods for the identification of PPIs (e.g., immunoprecipitation and affinity chromatography) are not suitable for determination of the strength of the interaction. For the target protein, this setup can be used for the screening of interacting proteins both for hit identification and characterization, while excluding the need for labeling of target protein(s).

To exclude the possibility of simultaneous binding of the probe and PKAr to PKAc, the lysate of cells co-expressing CFP-fused PKArII $\beta$  and YFP-fused PKAc $\alpha$  was used in a FRET assay. ARC-1411 ( $K_{D,PKAc} = 3$  pM) induced decrease of energy transfer from CFP to YFP as did the physiological activator cAMP, pointing to disruption of the PKA holoenzyme by both compounds.

Differently from the bisubstrate inhibitors ARC-1411 and ARC-902, ATP-competitive inhibitor H89 ( $K_{D,PKAc} = 10 \text{ nM}$ )<sup>33</sup> did not displace the regulatory subunit from the catalytic subunit. Furthermore, H89 induced the recovery of the holoenzyme after displacement of ARC-902 from the catalytic subunit. In cellular context, these results point to the fundamentally different effect of inhibitors targeted only to the ATP-pocket of PKAc (e.g., H89) and bifunctional inhibitors (e.g., ARC-902 and ARC-1411) on the PKA holoenzyme. We have previously shown that ARCs that comprise multiple D-arginine residues are proteolytically stable and well penetrate cell plasma membrane, thereafter localizing into cytoplasm and nuclei of mammalian cells.<sup>37</sup> Within cell environment, at higher concentration H89 can displace  $Mg_2ATP$  from PKA without disrupting the tetrameric PKA holoenzyme (nevertheless, stability of the holoenzyme is reduced). PKAc remains bound to PKArII and therefore localized to special regions of cell membranes *via* interaction of the latter protein dimer with AKAPs. In contrast, binding of a high-affinity ARC-inhibitor to the active site of PKAc leads to formation of ARC:PKAc complex and disruption of PPI between PKAc and PKAr (type I or type II subunit), relocating PKAc from the initial distinct cellular compartment as its anchoring to AKAP *via* PKAr is split. Free regulatory subunit PKAr may interact with other proteins, e.g., RSK1.<sup>49</sup> PKAc remains bound to the ARC-inhibitor, but the catalytically inactive complex is replaced from its native, AKAP-anchored position. Thus ARCs remove the inhibitor-bound PKAc from AKAP-rich regions, resembling to the specific PKA:AKAP interaction inhibitors that remove inactive PKA holoenzyme from the AKAP-rich region.<sup>50</sup> For both cases the feedback mechanism of adenylate cyclase (AC) inhibition by PKAc phosphorylation is disrupted, however the contrasting mechanism suggests different outcome within cell. Continuous production of cAMP can lead to activation of PKA dissociated by PKA:AKAP inhibitor, releasing PKAc for substrate phosphorylation events in remote locations. The inadequate control of activity by regulatory subunit is seen in the PKArII $\alpha$  overexpressing prostate cancer cells, in which application of PKI(6-22) peptide further improved the cell survival.<sup>51</sup> Considering that numerous AKAPs scaffold both AC and PKA, the application of ARCs emerge as a novel tool for studying the underlying mechanism of this important signaling pathway.

Although ARC-1411 revealed the superior binding affinity to PKAc ( $K_D = 3 \text{ pM}$ ), other ARCs in the set possess some prominent properties and may be preferred lead scaffolds for developing inhibitors of PPIs. Arrangement of the inhibitor and the protein in the complex ARC-1408:PKAc $\alpha$  points to efficiency of the technology of atom-wise fine-tuning of the



structure of a bifunctional inhibitor. ARC-1408 very well fits into the active site of PKA $\alpha$  (Figure 5A), forming numerous contacts with amino acid residues of both the ATP-binding pocket and protein-binding domain (or PPI interface) of the PK. ARC-1408 with MW of less than 800 D possesses impressively low  $K_D$  value of 180 pM towards PKAc. Although the MW of ARC-1408 exceeds the upper MW limit set by pharma companies for orally bioavailable small molecule drugs (MW = 500 D)<sup>46</sup>, many new compounds in different stages of clinical study have higher MW.<sup>52</sup> At the same time the affinity of ARC-1408 is higher than the inhibitory potency of AT13148<sup>53</sup>, a novel oral multi-AGC kinase inhibitor in clinical trials that inhibits PKs PKA ( $IC_{50}$  = 3 nM), AKT, p70S6K, ROCK, and most inhibitors of tyrosine kinases<sup>54</sup> approved as cancer drugs. It has been shown that inhibitors of enzymes and those of PPIs have a statistically significant difference in two out of five rules set for drugs (higher logP and MW) and only one third of inhibitors of PPI passed all five rules.<sup>55</sup> Although the average MW for the tested inhibitors of PPIs remained close to the limit of 500 Da, higher MW multiparmacophoric ligands promise to expand the druggable target library within interactome and are presumably an inevitable choice for inhibition of a selection of PPIs.

The results shown here encourage the further investigation of middle-sized bifunctional ligands that target a well-defined binding site of the protein in addition to the hot spot amino acid residues within the PPI interface as research tools for regulation of PPIs in biomedical studies and as candidates of future drugs.

## Methods

### Reagents

Chemicals from the following commercial sources were used: bovine serum albumin (BSA, Cahn Fraction V), dithiothreitol (DTT) from Fluka; ATP, Tween 20, and buffering reagents (Hepes, BisTris, Tris) from Sigma; NaCl and MgAc<sub>2</sub> from Riedel-de Haën; peptide synthesis reagents from Neosystem, Novabiochem, Advanced ChemTech, and AnaSpec; n-butylamine from Aldrich; Sypro Orange Protein Gel Stain and ROCKII from Invitrogen; AKT3 from KinaseDetect; organic solvents from Rathburn and Fluka; H89 (N-[2-[[3-(4-bromophenyl)-2-propenyl]amino]ethyl]-5-isoquinolinesulfonamide), cAMP-dependent protein kinase regulatory subunit I $\alpha$  (PKA $\alpha$ ), and full-length heat stable protein kinase inhibitor (PKI $\alpha$ , NP\_006814) from BIAffin.

### Equipment

The concentrations of stock solutions of ARC-type inhibitors and H89 were determined spectrophotometrically in aqueous buffer at pH 7.5 using a NanoDrop2000c. Molar extinction coefficients used for respective absorbing species: 13 000 M<sup>-1</sup>cm<sup>-1</sup> for ARC-1156 and ARC-1169 at 282 nm; 15 000 M<sup>-1</sup>cm<sup>-1</sup> at 260 nm for ARC-902; 16930 M<sup>-1</sup>cm<sup>-1</sup> at 276 nm for other purine analogue structures not incorporating a fluorescent marker; 250 000 M<sup>-1</sup>cm<sup>-1</sup> at 653 nm for Alexa Fluor 647-containing compound ARC-1063; 30 000 M<sup>-1</sup>cm<sup>-1</sup> at 260 nm for H89; 80 000 M<sup>-1</sup>cm<sup>-1</sup> at 559 nm for 5-TAMRA-containing ARC-1413; 70 000 M<sup>-1</sup>cm<sup>-1</sup> at 493 nm for Alexa Fluor 488-containing ARC-679.

Time-resolved (TR) measurement of luminescence intensity, steady-state measurement of fluorescence anisotropy (FA) and fluorescence intensity (FI) were performed with a PHERAstar microplate reader (BMG Labtech) using HTRF optic module [excitation 337(50) nm, emission 675(50) nm], FP optic module [excitation 540(20) nm, emission 590(20) nm], or FI optic module [excitation 427(10) nm, emission 530(10) nm and 480(10) nm], respectively.

ThermoFluor assay for determination of protein unfolding temperatures (using Boltzmann equation) were conducted using MiniOpticon Real-Time PCR detection system (BioRad) on Multiplate Low-Profile 48-Well Unskirted PCR Plates (BioRad) covered with Microseal C Optical Seals (BioRad). ThermoFluor experiments was controlled and the data recorded with Opticon Monitor software (Bio-Rad). Binding and displacement assays were performed on black, low-volume, 384-well, non-binding surface (NBS) microplates (cat. no. 3676, Corning). Thermo Scientific incubator was used to pre-heat the microplate and

samples to 30 °C for binding and displacement assays. GraphPad Prism (v5, GraphPad Software) was used for data analysis and PyMOL (The PyMOL Molecular Graphics Software v1.6, Schrodinger, LCC) for creation of crystal structure figures.

### *Synthesis of ARCs*

Peptide fragments were prepared on the Wang resin by using traditional Fmoc solid-phase peptide synthesis methods. After each step the resin was washed 5 times with DMF. Protected amino acids (3 Eq) were dissolved in DMF and activated with HBTU/HOBt (2.94 Eq each) and *N*-methylmorpholine (9 Eq) in DMF. After 3 minutes, the coupling solutions were added to the resin and shaken for 40–60 min at RT. The completeness of each coupling step was monitored with the Kaiser test.<sup>56</sup> Removal of Fmoc-group was performed with 20% piperidine solution in DMF (20 min). From synthesis methods tried, **Figure S1** represents the most successive pathway. In short, the respective dicarboxylic acid (10 Eq), HOBt (3 Eq), HBTU (3 Eq), and NMM (20 Eq) were dissolved in DMF. This ratio of the reagents led to predominant activation of a single carboxylic acid group of the  $\alpha,\omega$ -diacid and minimized the formation of crosslinked products. After 3 min, the coupling solutions were added to the resin and placed on orbital-shaker for 2 h at RT. Excess of reagents, HBTU (3 Eq), HOBt (3 Eq), and NMM (20 Eq) was dissolved in DMF and added to the resin for 40 minutes to activate the second carboxylic group of the diacid. After washing of the resin 5 times with DMF, the adenosine mimicking compound (1.5 Eq) was dissolved in DMF and added to the resin. Finally the resin was washed 5 times with each solvent (DMF, isopropanol, DCE) and dried. Treatment with TFA/H<sub>2</sub>O/triisopropylsilane (5/90/5 by volume) for 2 h was used as a standard cleavage procedure to get crude peptide conjugates that were purified by reverse phase HPLC and freeze-dried.

### *Time-resolved luminescence intensity displacement assay for affinity determination of synthesized compounds*

Displacement assay based on time-resolved (TR) measurement of luminescence intensity was used for determination of the affinity of synthesized compounds (detailed description in Enkvist *et al.*)<sup>26</sup>. The assay based on TR measurement of luminescence was chosen instead of FA-based assay mainly because of the possibility of using the probe ARC-1063 in excess compared to the PK, which is required for characterization of inhibitors with very high affinity. Briefly, TR luminescence intensity measurements were performed in the assay buffer [50 mM Hepes (pH = 7.5), 150 mM NaCl, 5 mM DTT, 0.5 mg/ml BSA] in final volumes of 20  $\mu$ l. Assay was carried out by preparation of the 3-fold titrations series

( $n = 1$ ) of the competitive inhibitor and a fixed concentration of PK:ARC-1063 complex was added to each well as follows (**Supporting Information, Part 4**): 1 nM PKA $\alpha$  with 50 nM ARC-1063 for ARC-1411, ARC-1413, ARC-1415, ARC-1416, and 2 nM ARC-1063 for inhibitors possessing lower affinity with PKA $\alpha$ ; 2.5 nM ROCKII with 5 nM ARC-1063 for ARC-1411, ARC-1412, ARC-1413, ARC-1415, ARC-1416, and 0.5 nM ARC-1063 for the remaining ARCs; 1 nM AKT3 with 50 nM ARC-1063 for ARC-1411, ARC-1413, and 3 nM AKT3 with 2 nM ARC-1063 with the remaining ARCs. Each set of measurements were accompanied with titration series of ARC-902 as a control. The incubation of the titration series were carried out at 30 °C for 1 h. The displacement curves were measured using HTRF optical module and the data were fitted to a sigmoidal dose-response model to obtain  $IC_{50}$  values.  $K_D$  values were calculated according to the equation

$$K_{D, \text{competitor}} = [I]_{50} / ([ARC-1063]_{50} / K_{D, \text{ARC-1063}} + [P]_0 / K_{D, \text{ARC-1063}} + 1)^{57}, \quad (1)$$

where  $[I]_{50}$  is the concentration of free inhibitor at 50% of displacement,  $[ARC-1063]_{50}$  is the concentration of probe at 50% of displacement,  $[P]_0$  is the concentration of free PK without the presence of competitor, and  $K_{D, \text{ARC-1063}}$  is the dissociation equilibrium constant of the probe towards the PK (15 pM for PKA $\alpha$ , 5 nM for AKT3, and 0.2 nM for ROCKII). The resulting  $K_D$  values were used for correlation with ThermoFluor measurements (**Figure 1**).

#### **Displacement assay with FA read-out for characterization of protein substrate-competitive inhibitors**

Displacement assay based on the measurement of fluorescence anisotropy (FA) was performed in the assay buffer [50 mM Hepes (pH = 7.5), 150 mM NaCl, 5 mM DTT, 0.5 mg/ml BSA] in the presence of 10  $\mu$ M ATP and 10 mM  $Mg^{2+}$  in final volumes of 20  $\mu$ l in wells of 384-well microtiter plates. The assay was performed by titrating fixed concentration of the complex of ARC-1413 (2 nM) and PKA $\alpha$  (3 nM) with PKA $\alpha$  or PKI (3-fold dilution series) and preincubated for 1.5 h at 30 °C. Measurements were conducted in parallels ( $n = 2$ ), for which standard error is depicted. Thereafter, 1.05  $\mu$ l of 1 mM cAMP was added to the titration series of PKA $\alpha$ , resulting in a total concentration of 50  $\mu$ M cAMP. The displacement curves were measured using the optical module for fluorescence polarization (FP) measurements [excitation 540(20) nm, emission 590(20) nm]. Resulting data were fitted to a sigmoidal dose response model to obtain  $IC_{50}$  values (**Figure 2**).  $K_D$  values were calculated by using the equation

$$K_{D, \text{competitor}} = [I]_{50} / ([ARC-1413]_{50} / K_{D, \text{ARC-1413}} + [P]_0 / K_{D, \text{ARC-1413}} + 1), \quad (2)$$

where  $K_{D, \text{ARC-1413}}$  is the dissociation equilibrium constant of the probe towards PKA $\alpha$

( $K_{D,ARC-1413} = 5.6$  pM),  $[I]_{50}$  is the concentration of free inhibitor at 50% of displacement,  $[ARC-1413]_{50}$  is the concentration of probe at 50% of displacement,  $[P]_0$  is the concentration of free PK without the presence of competitor.

### ***Dissociation kinetics of the complex ARC-1413:PKA $\alpha$***

Probe ARC-1413 (4 nM) and PKA $\alpha$  (6 nM) were mixed and incubated at 30 °C in a well of a microplate to a 10  $\mu$ l volume. Competitive inhibitor (10  $\mu$ l) ARC-1411 or ARC-902 was added to the mixture at  $t = 0$  s with the final concentration of 10  $\mu$ M or 75  $\mu$ M, respectively ( $n = 1$ ). The FA measurements were performed with 60 s increments over a time course of 1 h using the FP module of PHERAstar plate reader and the resulting data were fitted to the first-order kinetic model to obtain the dissociation rate constant ( $k_{off}$ ) for the inhibitor:PKA $\alpha$  complex:

$$mA = e^{-k_{off} \cdot t} \cdot (mA_{t=0} - mA_{plateau}) + mA_{plateau} \quad (3)$$

### ***Investigation of thermal stability effect of ARC-type inhibitors on PKs***

ThermoFluor measurements were carried out in buffer containing 50 mM Tris (pH = 7.5) and 50 mM NaCl in a final volume of 25  $\mu$ l<sup>58</sup>. Sypro Orange stock solution (5000x) was added to samples (dilution factor of 90) containing a fixed concentrations of PK (10  $\mu$ M, AKT3 protein used for ThermoFluor measurements was not fully activated) and the inhibitor (40  $\mu$ M). Wells were then sealed and the measurement of fluorescence intensity accompanied by temperature program in the range of 5–90 °C was initiated. Denaturation temperature of the PK was found from intensity and  $dI/dT$  data of triplicates ( $n = 3$ ), for which standard error bars are shown (please see **Figure S3**, PKA $\alpha$  data was further used for **Figure 1**).

### ***Protein expression and purification***

Untagged full-length human PKA $\alpha$  (UniProt accession no. P17612) was expressed in Escherichia coli BL21-(DE3) cells (Stratagene) from a construct based on the vector pET-28b(+) (Novagen) in Studier autoinduction medium<sup>59</sup>. The expression was carried out over a period of 24 h at 24 °C. The following procedure of protein purification was performed according to published descriptions.<sup>41</sup>

C9H6 cells stably expressing CFP-fused PKA regulatory subunit (PKA $\beta$ -L20-CFP) and YFP-fused PKA catalytic subunit (PKA $\alpha$ -YFP) were seeded on six-well Nunc plate (Thermo Scientific) and grown for up to 72 h<sup>37,38</sup>. Cells were lysed using NP-40 cell lysis buffer

(FNN0021, Life Technologies) containing 1x protease inhibitor cocktail (Complete EDTA free, Roche), 1% Triton X, 0.5 mM DTT and 0.5 mM phenylmethanesulfonyl fluoride (PMSF).

***Fluorescence intensity ratio experiments with C9H6 cell lysate containing fused proteins PKAII $\beta$ -L20-CFP and PKA $\alpha$ -YFP***

The approximate concentration of fused proteins was assessed by using a two-fold dilution series of C9H6 cell lysate in parallel to ARC-679 labelled with Alexa Fluor 488. For 5% of C9H6 lysate used in experiments, the concentration of fused proteins was approximately 5 nM (**Figure S5A**).

ARC-1411, ARC-902, and cAMP were serially three-fold diluted in assay buffer [50 mM Hepes (pH 7.5), 150 mM NaCl, and 0.005% Tween 20]. C9H6 cell lysate was then added to each well of the dilution series to a dilution of 5%. Duplicates ( $n = 2$ ) of displacement series were measured (standard error of the mean is depicted for the measurements) after incubation period of 1 h using FI optical module of PHERAstar plate reader [excitation at 427(10) nm, emission at 530(10) nm and 480(10) nm]. The resulting data were used to calculate relative FI ratio of signals in donor and acceptor channels in the absence and presence of the inhibitor based on the equation

$$\text{Relative FI ratio} = (I_a/I_d)/(I_{a,D}/I_{d,D}), \quad (4)$$

in which  $I_a$  and  $I_d$  denote the emission intensity in the acceptor and donor channels in the absence of a competitor, and  $I_{a,D}$  and  $I_{d,D}$  are the emission intensity in the acceptor and donor channel in the presence of the competitor, respectively. The ratio was fitted to sigmoidal dose response model to obtain  $IC_{50}$  values.

The effect of  $Mg^{2+}$  and ATP was measured ( $n = 1$ ) as described above in the presence of 100  $\mu$ M ATP and 10 mM  $Mg(CH_3COO)_2$ . Further, the lysate containing fused PKA holoenzyme with a final dilution of 5% was added to the ARC-1411 titration series (3-fold dilution), and series containing 10 mM  $Mg^{2+}$ , 100  $\mu$ M ATP and 10 mM  $Mg^{2+}$ , 100  $\mu$ M H89 and 10 mM  $Mg^{2+}$  were prepared ( $n = 1$ ) in parallel. These series were incubated for 1 h and measured as described above (**Figure S6A**). Following measurement, 20 mM EDTA was added to each well of each titration series and incubated for 1 h, followed by measurement of FI as previously (**Figure S6B**).

Experiments of dissociation kinetics were performed with 5% of C9H6 cell lysate containing PKAII $\beta$ -CFP and PKA $\alpha$ -YFP fusion proteins. Compound H89 or ARC-902 was added to the lysate with the final concentration of 50  $\mu$ M or 10  $\mu$ M, respectively, and FI optic

module [excitation 427(10) nm, emission 530(10) nm and 480(10) nm] was used for measuring the fluorescence intensity in 15 s intervals ( $n = 1$ ). The resulting intensity values for both channels can be found from **Figure S5D**. All reagents and the microplate were pre-incubated at 30 °C. The dissociation rate constant for the resulting time-dependent FI ratio data was calculated using the first-order kinetic model.

***Conditions for co-crystallization of recombinant PKA $\alpha$  with synthesized ARCs, diffraction data collection, and structure determination***

PKA $\alpha$  was transferred (spin column centrifugation) into crystallization buffer [25 mM BisTris (pH 7.0), 150 mM KCl] at concentration of 8 mg/ml. ARC compounds were subsequently added to the solution (final concentration of 1 mM). The PKA $\alpha$ :ARC-1411 complex was crystallized in 0.4 M Li<sub>2</sub>SO<sub>4</sub>, 0.1 M phosphate/0.1 M citrate (pH 4.5), 17-19% PEG 1500, at 4 °C. It cannot be ruled out that the packing of the PKA $\alpha$  molecules in the asymmetric unit or presence of oxyanions (sulfate/phosphate) displaces the ligands from their preferred binding mode, contributing to the observed flexibility (**Figure S7**). The PKA $\alpha$ :ARC-1408 complex was crystallized in 0.1 M BisTris (pH 7.0), 0.2 M (NH<sub>4</sub>)<sub>2</sub>SO<sub>4</sub>, and 20-24% PEG 3350 at 4 °C. In both cases the crystal quality was improved by streak seeding and Paratone-N was used for cryo-protection. The PKA $\alpha$ :ARC-1416 complex was successfully crystallized in 18% PEG3350, 0.2 M Li<sub>2</sub>SO<sub>4</sub> at 4 °C.

The diffraction of frozen crystals was measured at the “Berliner Elektronenspeicherring-Gesellschaft für Synchrotronstrahlung” (BESSY, Berlin, Germany) and at the European Synchrotron Radiation Facility (ESRF, Grenoble, France). The resulting data were integrated and scaled with the programs XDS<sup>60</sup> and XSCALE<sup>60</sup>, or MOSFLM<sup>61</sup> and SCALA<sup>62</sup> from the CCP4 package<sup>63</sup>. Molecular replacement and structure refinement were carried out with PHASER<sup>64</sup> and PHENIX refine<sup>65</sup>. Coordinate and molecular topology files for ligands were created with ELBOW<sup>65</sup> and PRODRG<sup>66</sup>.

1  
2  
3  
4  
5  
6  
7  
8  
9  
10  
11  
12  
13  
14  
15  
16  
17  
18  
19  
20  
21  
22  
23  
24  
25  
26  
27  
28  
29  
30  
31  
32  
33  
34  
35  
36  
37  
38  
39  
40  
41  
42  
43  
44  
45  
46  
47  
48  
49  
50  
51  
52  
53  
54  
55  
56  
57  
58  
59  
60

584       •   **ASSOCIATED CONTENT**

585           Supporting Information

586           Synthesis scheme, full structures, and characterization of synthesized inhibitors,  
587           additional information of biological characterization and crystal structures.

588       •   **ACCESSION CODES**

589           The PDB codes for the ARC-1408, ARC-1411, and ARC-1416 in complex with  
590           PKA $\alpha$  are 5IZF, 5IZJ, and 5J5X, respectively.

591       •   **AUTHOR INFORMATION**

592           \* Fax: +372 7375275. E-mail address: Asko.Uri@ut.ee (A. Uri).

593           The authors declare no competing financial interest.

594       •   **ACKNOWLEDGEMENTS**

595           This work was supported by grants from the Estonian Research Council (IUT20-17),  
596           the Estonian Ministry of Education and Sciences (SF0180121s08), and the Estonian  
597           Science Foundation (8230 and 8419). We thank the British Heart Foundation  
598           (PG/10/75/28537 and RG/12/3/29423) on behalf of M.Z. We are grateful for support  
599           from Norwegian Research Council Project 183376 (R.A.E., A.P.) and the Norwegian  
600           Research Council PhD school BioStruct (R.A.E., K.A.A.) for support.

601  
602       •   **AUTHOR CONTRIBUTIONS**

603           A.U. designed studies, discussed results, and contributed to writing of manuscript. T.I.  
604           wrote the bulk of the manuscript, contributed to the purification of compounds, and  
605           designed and performed biochemical measurements. E.E. contributed to design and  
606           synthesis of compounds. B.V. contributed to synthesis of compounds. G.b.M.  
607           contributed to biochemical measurements. G.R. contributed to purification of  
608           compounds. A.P. and K.A.A. performed crystallization and analyzed crystallographic  
609           data. M.Z. provided the C9H6 cells. R.A.E. contributed to crystal structure analysis.



## REFERENCES

- (1) Pastrello, C., Pasini, E., Kotlyar, M., Otasek, D., Wong, S., Sangrar, W., Rahmati, S., and Jurisica, I. (2014) Integration, visualization and analysis of human interactome. *Biochem. Biophys. Res. Commun.* *445*, 757–773.
- (2) Sheng, C., Dong, G., Miao, Z., Zhang, W., and Wang, W. (2015) State-of-the-art strategies for targeting protein-protein interactions by small-molecule inhibitors. *Chem Soc Rev* *44*, 8238–8259.
- (3) Ezkurdia, I., Juan, D., Rodriguez, J. M., Frankish, A., Diekhans, M., Harrow, J., Vazquez, J., Valencia, A., and Tress, M. L. (2014) Multiple evidence strands suggest that there may be as few as 19 000 human protein-coding genes. *Hum. Mol. Genet.* *23*, 5866–5878.
- (4) Arkin, M. R., Tang, Y., and Wells, J. A. (2014) Small-Molecule Inhibitors of Protein-Protein Interactions: Progressing toward the Reality. *Chem. Biol.* *21*, 1102–1114.
- (5) Chen, J., Sawyer, N., and Regan, L. (2013) Protein-protein interactions: General trends in the relationship between binding affinity and interfacial buried surface area. *Protein Sci.* *22*, 510–515.
- (6) Clackson, T., and Wells, J. A. (1995) A hot spot of binding energy in a hormone-receptor interface. *Science* *267*, 383–386.
- (7) Smith, M. C., and Gestwicki, J. E. (2012) Features of protein-protein interactions that translate into potent inhibitors: topology, surface area and affinity. *Expert Rev. Mol. Med.* *14*, e16.
- (8) Nim, S., Jeon, J., Corbi-Verge, C., Seo, M.-H., Ivarsson, Y., Moffat, J., Tarasova, N., and Kim, P. M. (2016) Pooled screening for antiproliferative inhibitors of protein-protein interactions. *Nat. Chem. Biol.* *12*, 275–281.
- (9) de Oliveira, P. S., Ferraz, F. A., Pena, D. A., Pramio, D. T., Morais, F. A., and Schechtman, D. (2016) Revisiting protein kinase-substrate interactions: Toward therapeutic development. *Sci. Signal.* *9*, re3.
- (10) Roskoski, R. (2015) A historical overview of protein kinases and their targeted small molecule inhibitors. *Pharmacol. Res.* *100*, 1–23.
- (11) Sharma, S., Singh, J., Ojha, R., Singh, H., Kaur, M., Bedi, P. M. S., and Nepali, K. (2016) Design strategies, structure activity relationship and mechanistic insights for purines as kinase inhibitors. *Eur. J. Med. Chem.* *112*, 298–346.
- (12) Lievens, S., Gerlo, S., Lemmens, I., De Clercq, D. J. H., Risseuw, M. D. P., Vanderroost, N., De Smet, A.-S., Ruysinck, E., Chevet, E., Van Calenbergh, S. *et al.* (2014) Kinase Substrate Sensor (KISS), a mammalian in situ protein interaction sensor. *Mol. Cell. Proteomics* *13*, 3332–42.
- (13) Kung, J. E., and Jura, N. (2016) Structural Basis for the Non-catalytic Functions of Protein Kinases. *Structure* *24*, 7–24.
- (14) Claus, J., Cameron, A. J. M., and Parker, P. J. (2013) Pseudokinase drug intervention: a potentially poisoned chalice. *Biochem. Soc. Trans.* *41*, 1083–8.
- (15) Taylor, S. S., Yang, J., Wu, J., Haste, N. M., Radzio-Andzelm, E., and Anand, G. (2004) PKA: A portrait of protein kinase dynamics. *Biochim. Biophys. Acta - Proteins Proteomics* *1697*, 259–269.
- (16) Herberg, F. W., Maleszka, A., Eide, T., Vossebein, L., and Tasken, K. (2000) Analysis of A-kinase anchoring protein (AKAP) interaction with protein kinase A (PKA) regulatory subunits: PKA isoform specificity in AKAP binding. *J. Mol. Biol.* *298*, 329–339.
- (17) Herberg, F. W., and Taylor, S. S. (1993) Physiological inhibitors of the catalytic subunit of cAMP-dependent protein kinase: Effect of MgATP on protein-protein interactions. *Biochemistry* *32*, 14015–14022.
- (18) Enkvist, E., Lavogina, D., Raidaru, G., Vaasa, A., Viil, I., Lust, M., Viht, K., and Uri, A. (2006) Conjugation of adenosine and hexa-(D-arginine) leads to a nanomolar bisubstrate-

- 660 analog inhibitor of basophilic protein kinases. *J. Med. Chem.* 49, 7150–9.
- 661 (19) Gower, C. M., Chang, M. E. K., and Maly, D. J. (2014) Bivalent inhibitors of protein  
662 kinases. *Crit. Rev. Biochem. Mol. Biol.* 49, 102–115.
- 663 (20) Jencks, W. P. (1981) On the attribution and additivity of binding energies. *Proc. Natl.*  
664 *Acad. Sci. U. S. A.* 78, 4046–50.
- 665 (21) Lavogina, D., Enkvist, E., and Uri, A. (2010) Bisubstrate inhibitors of protein kinases:  
666 from principle to practical applications. *ChemMedChem* 5, 23–34.
- 667 (22) Lavogina, D., Kestav, K., Chaikuad, A., Heroven, C., Knapp, S., and Uri, A. (2016) Co-  
668 crystal structures of the protein kinase haspin with bisubstrate inhibitors. *Acta Crystallogr. Sect.*  
669 *F Struct. Biol. Commun.* 72, 339–345.
- 670 (23) Pflug, A., Rogozina, J., Lavogina, D., Enkvist, E., Uri, A., Engh, R. A., and Bossemeyer,  
671 D. (2010) Diversity of bisubstrate binding modes of adenosine analogue-oligoarginine  
672 conjugates in protein kinase a and implications for protein substrate interactions. *J. Mol. Biol.*  
673 403, 66–77.
- 674 (24) Vaasa, A., Viil, I., Enkvist, E., Viht, K., Raidaru, G., Lavogina, D., and Uri, A. (2009)  
675 High-affinity bisubstrate probe for fluorescence anisotropy binding/displacement assays with  
676 protein kinases PKA and ROCK. *Anal. Biochem.* 385, 85–93.
- 677 (25) Lavogina, D., Lust, M., Viil, I., König, N., Raidaru, G., Rogozina, J., Enkvist, E., Uri, A.,  
678 and Bossemeyer, D. (2009) Structural analysis of ARC-type inhibitor (ARC-1034) binding to  
679 protein kinase A catalytic subunit and rational design of bisubstrate analogue inhibitors of  
680 basophilic protein kinases. *J. Med. Chem.* 52, 308–21.
- 681 (26) Enkvist, E., Vaasa, A., Kasari, M., Kriisa, M., Ivan, T., Ligi, K., Raidaru, G., and Uri, A.  
682 (2011) Protein-induced long lifetime luminescence of nonmetal probes. *ACS Chem. Biol.* 6,  
683 1052–62.
- 684 (27) Pantoliano, M. W., Petrella, E. C., Kwasnoski, J. D., Lobanov, V. S., Myslik, J., Graf, E.,  
685 Carver, T., Asel, E., Springer, B. A., Lane, P. *et al.* (2001) High-density miniaturized thermal  
686 shift assays as a general strategy for drug discovery. *J. Biomol. Screen. Off. J. Soc. Biomol.*  
687 *Screen.* 6, 429–440.
- 688 (28) Chijiwa, T., Mishima, A., Hagiwara, M., Sano, M., Hayashi, K., Inoue, T., Naito, K.,  
689 Toshioka, T., and Hidaka, H. (1990) Inhibition of forskolin-induced neurite outgrowth and  
690 protein phosphorylation by a newly synthesized selective inhibitor of cyclic AMP-dependent  
691 protein kinase, N-[2-(p-bromocinnamylamino)ethyl]-5-isoquinolinesulfonamide (H-89), of  
692 PC12D pheochromocytoma. *J. Biol. Chem.* 265, 5267–5272.
- 693 (29) Fedorov, O., Marsden, B., Pogacic, V., Rellos, P., Müller, S., Bullock, A. N., Schwaller,  
694 J., Sundström, M., and Knapp, S. (2007) A systematic interaction map of validated kinase  
695 inhibitors with Ser/Thr kinases. *Proc. Natl. Acad. Sci. U. S. A.* 104, 20523–20528.
- 696 (30) Fedorov, O., Niesen, F. H., and Knapp, S. (2012) Kinase inhibitor selectivity profiling  
697 using differential scanning fluorimetry. *Methods Mol. Biol.* 795, 109–18.
- 698 (31) Matulis, D., Kranz, J. K., Salemme, F. R., and Todd, M. J. (2005) Thermodynamic stability  
699 of carbonic anhydrase: measurements of binding affinity and stoichiometry using ThermoFluor.  
700 *Biochemistry* 44, 5258–66.
- 701 (32) Lo, M. C., Aulabaugh, A., Jin, G., Cowling, R., Bard, J., Malamas, M., and Ellestad, G.  
702 (2004) Evaluation of fluorescence-based thermal shift assays for hit identification in drug  
703 discovery. *Anal. Biochem.* 332, 153–159.
- 704 (33) Viht, K., Schweinsberg, S., Lust, M., Vaasa, A., Raidaru, G., Lavogina, D., Uri, A., and  
705 Herberg, F. W. (2007) Surface-plasmon-resonance-based biosensor with immobilized  
706 bisubstrate analog inhibitor for the determination of affinities of ATP- and protein-competitive  
707 ligands of cAMP-dependent protein kinase. *Anal. Biochem.* 362, 268–77.
- 708 (34) Walsh, D. A., Ashby, C. D., Gonzalez, C., Calkins, D., Fischer, E. H., and Krebs, E. G.  
709 (1971) Purification and Characterization of a Protein Inhibitor of Adenosine 3',5'-

- Monophosphate-dependent protein kinases. *J. Biol. Chem.* 246, 1977-1985.
- (35) Dalton, G. D., and Dewey, W. L. (2006) Protein kinase inhibitor peptide (PKI): A family of endogenous neuropeptides that modulate neuronal cAMP-dependent protein kinase function. *Neuropeptides* 40, 23–34.
- (36) Cheung, J., Ginter, C., Cassidy, M., Franklin, M. C., Rudolph, M. J., Robine, N., Darnell, R. B., and Hendrickson, W. a. (2015) Structural insights into mis-regulation of protein kinase A in human tumors. *Proc. Natl. Acad. Sci.* 112, 1374–1379.
- (37) Vaasa, A., Lust, M., Terrin, A., Uri, A., and Zacco, M. (2010) Small-molecule FRET probes for protein kinase activity monitoring in living cells. *Biochem. Biophys. Res. Commun.* 397, 750–755.
- (38) Lissandron, V., Terrin, A., Collini, M., D’Alfonso, L., Chirico, G., Pantano, S., and Zacco, M. (2005) Improvement of a FRET-based indicator for cAMP by linker design and stabilization of donor-acceptor interaction. *J. Mol. Biol.* 354, 546–555.
- (39) Zawadzki, K. M. (2003) cAMP-dependent Protein Kinase Regulatory Subunit Type II : Active Site Mutations Define an Isoform-Specific Network for Allosteric Signaling by cAMP. *J. Biol. Chem.* 279, 7029–7036.
- (40) Kim, J., Li, G., Walters, M. A., Taylor, S. S., and Veglia, G. (2016) Uncoupling Catalytic and Binding Functions in the Cyclic AMP-Dependent Protein Kinase A. *Structure* 3, 353–363.
- (41) Engh, R. A., Girod, A., Kinzel, V., Huber, R., and Bossemeyer, D. (1996) Crystal structures of catalytic subunit of cAMP-dependent protein kinase in complex with isoquinolinesulfonyl protein kinase inhibitors H7, H8, and H89. *J. Biol. Chem.* 271, 26157–26164.
- (42) Pflug, A., Johnson, K. A., and Engh, R. A. (2012) Anomalous dispersion analysis of inhibitor flexibility: a case study of the kinase inhibitor H-89. *Acta Crystallogr. Sect. F. Struct. Biol. Cryst. Commun.* 68, 873–7.
- (43) Cheng, X., Phelps, C., and Taylor, S. S. (2001) Differential binding of cAMP-dependent protein kinase regulatory subunit isoforms Ialpha and Ibeta to the catalytic subunit. *J. Biol. Chem.* 276, 4102–4108.
- (44) Zhang, P., Knape, M. J., Ahuja, L. G., Keshwani, M. M., King, C. C., Sastri, M., Herberg, F. W., and Taylor, S. S. (2015) Single Turnover Autophosphorylation Cycle of the PKA RIIB Holoenzyme. *PLOS Biol.* 13, e1002192.
- (45) Zheng, J., Knighton, D. R., Xuong, N. H., Taylor, S. S., Sowadski, J. M., and Ten Eyck, L. F. (1993) Crystal structures of the myristylated catalytic subunit of cAMP-dependent protein kinase reveal open and closed conformations. *Protein Sci.* 2, 1559–73.
- (46) Veber, D. F., Johnson, S. R., Cheng, H.-Y., Smith, B. R., Ward, K. W., and Kopple, K. D. (2002) Molecular properties that influence the oral bioavailability of drug candidates. *J. Med. Chem.* 45, 2615–23.
- (47) Ohkanda, J. (2013) Module assembly for designing multivalent mid-sized inhibitors of protein-protein interactions. *Chem. Rec.* 13, 561–575.
- (48) Xinyi Huang. (2003) Fluorescence Polarization Competition Assay: The Range of Resolvable Inhibitor Potency Is Limited by the Affinity of the Fluorescent Ligand. *J. Biomol. Screen.* 8, 34–38.
- (49) Houslay, M. D. (2006) A RSK(y) relationship with promiscuous PKA. *Sci. STKE* 349, pe32.
- (50) Dema, A., Perets, E., Schulz, M. S., Deák, V. A., and Klusmann, E. (2015) Pharmacological targeting of AKAP-directed compartmentalized cAMP signalling. *Cell. Signal.* 27, 2474–2487.
- (51) Zynda, E. R., Matveev, V., Makhanov, M., Chenchik, A., and Kandel, E. S. (2014) Protein kinase A type II-alpha regulatory subunit regulates the response of prostate cancer cells to taxane treatment. *Cell Cycle* 13, 3292–3301.

- (52) Besbes, S., Pocard, M., Mirshahi, M., and Billard, C. (2016) The first MCL-1-selective BH3 mimetics have therapeutic potential for chronic lymphocytic leukemia. *Crit. Rev. Oncol. Hematol* 100, 32–36.
- (53) Yap, T. A., Walton, M. I., Grimshaw, K. M., te Poele, R. H., Eve, P. D., Valenti, M. R., de Haven Brandon, A. K., Martins, V., Zetterlund, A., Heaton, S. P. *et al.* (2012) AT13148 Is a Novel, Oral Multi-AGC Kinase Inhibitor with Potent Pharmacodynamic and Antitumor Activity. *Clin. Cancer Res.* 18, 3912–3923.
- (54) Hojjat-Farsangi, M. (2014) Small-molecule inhibitors of the receptor tyrosine kinases: promising tools for targeted cancer therapies. *Int. J. Mol. Sci.* 15, 13768–13801.
- (55) Villoutreix, B. O., Labbé, C. M., Lagorce, D., Laconde, G., and Sperandio, O. (2012) A leap into the chemical space of protein-protein interaction inhibitors. *Curr. Pharm. Des.* 18, 4648–67.
- (56) Kaiser, E., Colescott, R. L., Bossinger, C. D., and Cook, P. I. (1970) Color test for detection of free terminal amino groups in the solid-phase synthesis of peptides. *Anal. Biochem.* 34, 595–8.
- (57) Nikolovska-Coleska, Z., Wang, R., Fang, X., Pan, H., Tomita, Y., Li, P., Roller, P. P., Krajewski, K., Saito, N. G., Stuckey, J. A. *et al.* (2004) Development and optimization of a binding assay for the XIAP BIR3 domain using fluorescence polarization. *Anal. Biochem.* 332, 261–273.
- (58) Ericsson, U. B., Hallberg, B. M., DeTitta, G. T., Dekker, N., and Nordlund, P. (2006) Thermofluor-based high-throughput stability optimization of proteins for structural studies. *Anal. Biochem.* 357, 289–298.
- (59) Studier, F. W. (2005) Protein production by auto-induction in high density shaking cultures. *Protein Expr. Purif.* 41, 207–34.
- (60) Kabsch, W. (2010) Xds. *Acta Crystallogr. Sect. D Biol. Crystallogr.* 66, 125–132.
- (61) Leslie, A. G. W., and Powell, H. R. Processing diffraction data with MOSFLM. *Evol. Methods Macromol. Crystallogr. Struct. PATH TO Underst. Mech. ACTION CBRN AGENTS* 245, 41–51.
- (62) Evans, P. (2006) Scaling and assessment of data quality. *Acta Crystallogr. Sect. D Biol. Crystallogr.* 62, 72–82.
- (63) Collaborative Computational Project Number 4. (1994) The CCP4 suite: programs for protein crystallography. *Acta Crystallogr. D. Biol. Crystallogr.* D50, 760–3.
- (64) McCoy, A. J., Grosse-Kunstleve, R. W., Adams, P. D., Winn, M. D., Storoni, L. C., and Read, R. J. (2007) Phaser crystallographic software. *J. Appl. Crystallogr.* 40, 658–674.
- (65) Adams, P. D., Afonine, P. V., Bunkóczi, G., Chen, V. B., Davis, I. W., Echols, N., Headd, J. J., Hung, L. W., Kapral, G. J., Grosse-Kunstleve, R. W. *et al.* (2010) PHENIX: A comprehensive Python-based system for macromolecular structure solution. *Acta Crystallogr. Sect. D Biol. Crystallogr.* 66, 213–221.
- (66) Schüttelkopf, A. W., and Van Aalten, D. M. F. (2004) PRODRG: A tool for high-throughput crystallography of protein-ligand complexes. *Acta Crystallogr. Sect. D Biol. Crystallogr.* 60, 1355–1363.